water

MDPI

Article

Improved Performance of Sulfur-Driven Autotrophic Denitrification Process by Regulating Sulfur-Based Electron Donors

Jiang Xu [1,2], Zhikun Lu [1,2], Yifeng Xu [1,2], Chuanzhou Liang [1,2] and Lai Peng [1,2,*]

1 Hubei Key Laboratory of Mineral Resources Processing and Environment, Wuhan University of Technology, Luoshi Road 122, Wuhan 430070, China; 320876@whut.edu.cn (J.X.); 293747@whut.edu.cn (Z.L.); yifeng.xu@whut.edu.cn (Y.X.); liangchuanzhou@whut.edu.cn (C.L.)

2 School of Resources and Environmental Engineering, Wuhan University of Technology, Luoshi Road 122, Wuhan 430070, China

* Correspondence: lai.peng@whut.edu.cn

Abstract: Sulfur-driven autotrophic denitrification (SADN) has demonstrated efficacy in nitrate (NO_3^-) removal from the aquatic environment. However, the insolubility of elemental sulfur (S^0) (maximum 5 μg/L at 25 °C) limited the NO_3^- removal rate. In this study, we investigated the performance of a laboratory-scale S^0-packed bed reactor (S^0-PBR) under various volumetric NO_3^- loading rates. By filling with smaller S^0 particles (0.5–1 mm) and introducing chemical sulfide (30–50 mg S^{2-}-S/L), a high NO_3^- removal rate (1.44 kg NO_3^--N/(m^3·d)) was achieved, which was substantially higher than previously reported values in SADN systems. The analysis of the average specific NO_3^- removal rates and the half-order kinetic constants jointly confirmed that the denitrification performance was significantly enhanced by decreasing the S^0 particle sizes from 10–12 mm to 1–2 mm. The smaller S^0 particles with a larger specific surface area improved the mass-transfer efficiency. Dosing chemical S^{2-} (20 mg S^{2-}-S/L) to trigger the abiotic polysulfuration process increased the specific NO_3^- removal rate from 0.366 to 0.557 g NO_3^--N/g VSS/h and decreased the portion of removed NO_3^--N in the form of nitrous oxide (N_2O-N) from 1.6% to 0.7% compared to the S^{2-}-free group.

Keywords: autotrophic denitrification; elemental sulfur; particles size; sulfide; polysulfuration process; nitrous oxide

check for updates

Citation: Xu, J.; Lu, Z.; Xu, Y.; Liang, C.; Peng, L. Improved Performance of Sulfur-Driven Autotrophic Denitrification Process by Regulating Sulfur-Based Electron Donors. *Water* **2024**, *16*, 730. https://doi.org/10.3390/w16050730

Academic Editors: Francesca Raganati and Alessandra Procentese

Received: 29 January 2024
Revised: 21 February 2024
Accepted: 22 February 2024
Published: 29 February 2024

1. Introduction

The widespread use of nitrogenous fertilizers in agriculture and inadequate wastewater treatment has significantly increased nitrate (NO_3^-) pollution in aquatic environments [1]. Zhang et al. (2021c) [2] measured NO_3^- data from 71 major rivers in 30 provinces in China, revealing that the NO_3^- concentration in approximately 8% of rivers exceeded the World Health Organization limit of 10 mg NO_3^--N/L [3]. The increasing NO_3^- loading to coastal zones has induced a severe algae boom, leading to the formation of a "dead zone" [4]. NO_3^- can be converted into nitrite (NO_2^-) or nitrosoamines in the esophagus, which easily aroused methemoglobinemia, blue-baby syndrome, carcinoma, and mutation, thereby posing a severe threat to human life and health [5,6]. Traditional physical/chemical methods (e.g., reverse osmosis, ion exchange, and electrodialysis) for NO_3^- removal from wastewater have drawbacks such as high operational cost, low selectivity, and the generation of secondary brine wastes [7].

Alternatively, the biological denitrification process was considered an effective approach for removing NO_3^-. During this process, NO_3^- was sequentially reduced to NO_2^-, nitric oxide (NO), nitrous oxide (N_2O), and di-nitrogen (N_2) [8]. Organic matters were the most commonly used electron donors to perform heterotrophic denitrification (HD), while

hydrogen (H_2), elemental sulfur (S^0), and iron compounds were utilized by autotrophic denitrifiers [7]. In practice, both insufficient and excessive supplements of organic matter in the HD process would result in poor performance of NO_3^- removal and organic residue in the effluent, respectively [9]. Organic supplementation increased the cost and caused biofouling due to the high production of biomass sludge [10].

The autotrophic denitrification process can potentially replace HD because of negligible residual organics in an effluent, given that inorganic matters are utilized as electron donors [10]. Autotrophic denitrifiers exhibited lower biomass production due to the lower biomass yields of 0.4–0.57 g VSS/g NO_3^--N [11] than 0.8–1.2 g VSS/g NO_3^--N for heterotrophic denitrifiers [12]. The sophisticated hydrogen-delivering systems involved high operating and maintenance costs, which hindered the application of hydrogen-driven autotrophic denitrification [13]. Recently, sulfur-driven autotrophic denitrification (SADN) with the stoichiometry shown as follows [14] (Equation (1)) has gained increasing attention because S^0 was non-toxic, readily available, and chemically stable under normal conditions and could be used "on demand" without overdosing concerns [15]. The yields (Y) of SADN were relatively low, 0.24 g COD/COD [16], resulting in substantial sludge reduction. SADN was more economical than HD, with estimated costs of \$0.45/per kg·N removed versus \$1.05/per kg·N removed [17]. In addition, N_2O, as an intermediate product during the biological denitrification process, is a potent greenhouse gas with approximately 300 times the global warming potential of carbon dioxide (CO_2) [18]. Less N_2O is produced in the SADN process [19].

$$1.1S^0 + NO_3^- + 0.76H_2O + 0.4CO_2 + 0.08NH_4^+ \rightarrow 0.08C_5H_7O_2N + 1.1SO_4^{2-} + 0.5N_2 + 1.28H^+ \quad (1)$$

The orthorhombic α-S_8^0, as the only steady form of S^0 under ambient conditions, was hardly soluble in water (5 µg/L, 25 °C) due to the high bond strength between S-S bonds in S_8^0-rings and its large molecular size [20]. Owing to this problem, the bioavailability of S^0 is too poor for sulfur-respiring bacteria, such as S^0-oxidizing bacteria (S^0OB) and S_8^0-reducing bacteria (S^0RB). Preliminary microbial hydrolysis of S^0 was required as S^0 was only taken up by sulfur-respiring bacteria after its solubilization [16,21,22]. The low solubility resulted in lower kinetics than the conventional HD or sulfate (SO_4^{2-}) reduction process, which could be seen as the main bottleneck preventing the S^0-driven bioprocess from realistic applications. Some studies demonstrated a positive relationship between the denitrification rate and factors affecting the surface area of S^0, including S^0 concentration [10], particle morphology [23], and size [24,25]. Additionally, the bioavailability of biogenic sulfur (S_{bio}^0) particles is superior to chemical sulfur (S_{chem}^0) due to its micro-crystallinity structure and higher specific area [26,27].

The nucleophilic attack between sulfide (S^{2-}) and S^0 under neutral or alkaline conditions results in the cleavage of S_8^0 rings and the formation of polysulfide (S_n^{2-}) as detailed in Equation (2) [20]. This chemical reaction has received much attention due to the higher solubility and bioavailability of S_n^{2-} [20,28,29]. Therefore, the polysulfide-involved SADN (PiSADN) process (Equation (3)) might be an effective method for realizing high-rate NO_3^- removal. However, the main challenge is how to continuously generate S_n^{2-} in situ. Although promoting the sulfidogenic bacteria activity for S^0/SO_4^{2-} reduction to trigger the polysulfuration process was an option [30], organic supplementation might lead to a failure of the SADN system because the faster growth rate of heterotrophic NO_3^--reducing bacteria than autotrophic NO_3^--reducing bacteria [31]. Interestingly, a recent study by Qiu et al. (2022) [32] proposed a novel PiSADN process for S^0-packed bed reactor (S^0-PBR), and the polysulfuration was induced by an autotrophic biological sulfur disproportionation (SD) process (Equation (4)). It was difficult to continuously obtain the precursor biogenic S^{2-} through the SD process because the reaction was thermodynamically unfavored under standard conditions [33]. The novel PiSADN process was only adaptable for low-strength

wastewater treatment and required sufficient alkalinity supplementation and complex internal recirculation devices.

$$HS^- + \frac{n-1}{8}S_8{}^0 \leftrightarrow S_n{}^{2-} + H^+ \quad (2)$$

$$S_n{}^{2-} + 6NO_3{}^- + 2H_2O \rightarrow S_{n\text{-}5}{}^{2-} + 5SO_4{}^{2-} + 3N_2 + 4H^+ \quad (3)$$

$$4S^0 + 4H_2O \rightarrow SO_4{}^{2-} + 3HS^- + 5H^+ \quad (4)$$

As stated above, soluble $S_n{}^{2-}$ remarkably enhances the bioavailability of S^0 and thus facilitates the $NO_3{}^-$ removal performance in the SADN system. However, there are many challenges in the generation pathways for precursor biogenic S^{2-}. Dosing organic matter in the SADN system poses a risk to the stability of the microbial community. The SD process is endergonic and is easily inhibited by the presence of high $NO_3{}^-$ loading. These concerns have hindered the development of high-rate in situ PiSADN applications. As such, we investigated the feasibility of establishing an in situ PiSADN system by adding chemical S^{2-} directly for the treatment of high-loading wastewater. Moreover, although the literature found that S^0 particle size was a key factor affecting the denitrification rate, the underlying kinetic mechanisms were not fully understood. Therefore, a laboratory-scale S^0-PBR was continuously operated for 163 days under different volumetric loading rates of $NO_3{}^-$. A laboratory-scale S^0-PBR was continuously operated for 163 days under different volumetric loading rates of $NO_3{}^-$. The specific aims of this study were to (a) demonstrate the feasibility of achieving a high $NO_3{}^-$ removal rate in the long-term S^0-PBR by introducing smaller S^0 particles and chemical S^{2-}; (b) investigate the effect of different S^0 particle sizes and S^{2-} initial concentrations on $NO_3{}^-$ removal, $NO_2{}^-$ accumulation, and N_2O production; and (c) analyze the underlying mechanisms of optimized $NO_3{}^-$ removal in the bioreactor. This work might facilitate a better understanding of how to achieve an efficient SADN process in the S^0-PBR.

2. Materials and Methods

2.1. Bioreactor Setup and Operation

A laboratory-scale plexiglass S^0-PBR (dimension: 8 cm diameter × 40 cm height) was operated under anaerobic conditions with an effective volume of 1.55 L. The outlet was set at 36 cm from the base. The S^0-PBR was covered with aluminum foil to prevent the growth of phototrophic bacteria during the entire operation period. The sample port with a 0.8 cm diameter was set at a height of 30 cm, while the bottom of the S^0-PBR was provided with an outlet port (2 cm diameter). Two peristaltic pumps (KCM-B146, Kamoer, Shanghai, China) were used in the S^0-PBR operation, i.e., one for feeding and the other for suction.

The S^0-PBR was filled with $S_{chem}{}^0$ (0.5–1 mm) and activated carbon (0.5–1 mm) particles with a volume ratio of around 2/3 and 1/3. The inoculation sludge was obtained from the aeration tank of a municipal wastewater treatment plant (Tangxun Lake wastewater treatment plant, Wuhan, China), and the total inoculum mass was approximately 5.4 g. The bioreactor was operated continuously in an up-flow mode at 25 ± 2 °C in a temperature-controlled room.

The S^0-PBR was fed with synthetic wastewater, as per Qiu et al. (2020) [30]. A step-wise increase in influent volumetric loading, 0.06 kg $NO_3{}^-$-N/(m^3·d) to 1.92 kg $NO_3{}^-$-N/(m^3·d), was achieved in Stage I (days 1–127) by increasing the $NO_3{}^-$ concentration of 20 to 400 mg $NO_3{}^-$-N and decreasing the hydraulic retention time (HRT). The influent flow rate was increased from 3.23 mL/min to 5.17 mL/min by adjusting the feeding pump, and accordingly, the HRT decreased from 8 h to 5 h. In Stage II (days 128–151), the chemical S^{2-} solution was provided into the S^0-PBR while maintaining the same influent $NO_3{}^-$ loading rate as the latter Stage I (days 100–127). In Stage III (days 156–163), the working conditions of the S^0-PBR were identical to the latter Stage I while ceasing the supplement of chemical S^{2-}. Sufficient $NaHCO_3$ was added to the synthetic wastewater, acting as an

alkalinity source and inorganic carbon for S^0OB growth. The details of the three operational conditions are presented in Table 1.

Table 1. Operational conditions of the S^0-PBR.

Stages	Stage I	Stage II	Stage III
NO_3^--N (mg/L)	20–400	400	400
HRT (h)	8–5	5	5
Loading (kg NO_3^--N/(m^3·d))	0.06–1.92	1.92	1.92
S^{2-} (mg S/L)	-	30–50	-

2.2. Batch Experiments

To investigate the appropriate S^0 particle size, Test I was performed in 100 mL serum bottles placed in a chamber (20 °C, 200 rpm), including four groups with different S^0 sizes, i.e., 10–12 mm, 7–9 mm, 3–5 mm, and 1–2 mm, respectively. All bottles were sealed with butyl rubber stoppers and purged with N_2 to obtain anaerobic conditions. The sludge was taken from the S^0-PBR, and the concentration in each bottle was 0.445 g MLVSS/L. A total of 50 mg NO_3^--N/L and 1 g S^0 particles with the above-mentioned different sizes were added. The purpose of providing excessive S^0 was to avoid the impact of S^0 limitation on the denitrification process. In addition, 2 g/L $NaHCO_3$ was provided to balance the pH and support the bacterial growth. The trace elements were the same as the S^0-PBR feed solution. The batch test was conducted in duplicate for 34 h, during which samples were taken at 0 h, 3 h, 6 h, 9.5 h, 12 h, 21.5 h, and 34 h to measure NO_3^- and NO_2^-.

As mentioned above, insoluble S^0 would be converted into soluble S_n^{2-} in the presence of S^{2-} at alkaline conditions. Based on this point, Test II was launched to investigate whether S_n^{2-} could promote the SADN process. Two sets of experiments with the presence of 0 and 20 mg S/L chemical S^{2-} were performed in different serum bottles containing 1 g S^0 particles (1–2 mm) and 0.473 g/L MLVSS. Controls lacking S^{2-} to monitor the conventional SADN process with S^0 as the only electron donor. This test lasted for 32 h, during which samples were collected at 0 h, 6 h, 9.5 h, 22 h, 27.5 h, and 32 h to measure NO_3^-, NO_2^-, N_2O, and S^{2-} concentrations. Other operational conditions were the same as those mentioned above.

2.3. Chemical Analysis

The NO_3^-, NO_2^-, S^{2-} and SO_4^{2-} in the water samples were measured after filtering using disposable Millipore filter units (pore size: 0.22 μm). NO_3^- and NO_2^- were measured using an ultraviolet–visible spectrophotometer (UV5500PC, Shanghai Metash Instruments Co., Ltd., Shanghai, China). Dissolved N_2O in water samples was analyzed using a gas chromatograph (7890 plus GC, Lunan Ruihong Chemical Instrument, Tengzhou, Shandong, China) fitted with an HP-Plot Molesieve column (30 m × 0.53 mm × 25 μm) and an electron capture detector (ECD). SO_4^{2-} was quantified using an ion chromatograph (883 Basic IC plus, Metrohm, Switzerland) with a conductivity detector. Total dissolved sulfide (H_2S, HS^-, and S^{2-}) was determined using the methylene blue method [34]. The concentration of S_n^{2-} was indicated by the dissolved zero-valent sulfur atoms in polysulfide ions, which was measured by the above UV at a wavelength of 285 nm after filtration [35,36]. pH and temperature were measured with portable meters (Multi-Parameter Meter, HQ40D, Hach, Loveland, CO, USA). MLSS and MLVSS in the sludge used in batch tests were determined according to APHA (2005) [34].

3. Results and Discussion

3.1. Optimization of the S^0-PBR Performance

To enhance the S^0-PBR performance, a long-term continuous-flow experiment focused on reducing the size of S_{chem}^0 particles and facilitating the formation of S_n^{2-}. Three opera-

tional conditions were applied in the bioreactor. In Stage I, the S_{chem}^0 particles (0.5–1 mm) were used as the main filler. The volumetric loading rate of the reactor was step-wise increased to investigate the feasibility of enhancing NO_3^- removal capability by reducing S_{chem}^0 particle size in S^0-PBR. In Stage II, on the basis of optimum S_{chem}^0 particle size, the chemical precursor S^{2-} (30–50 mg S^{2-}-S/L) was added to form S_n^{2-} to accelerate the SADN process. In Stage III, the external S^{2-} addition was completely eliminated so that the polysulfuration process was inhibited, highlighting the positive effect of S_n^{2-} as an electron donor on the SADN process.

In Stage I (day 1–127), the influent NO_3^- concentration increased from 20 to 400 mg NO_3^--N/L, and HRT decreased from 8 h to 5 h, resulting in a step-wise increase in volumetric loading rate from 0.06 kg NO_3^--N/(m^3·d) to 1.92 kg NO_3^--N/(m^3·d). Of note, even with an influent NO_3^- loading as low as 0.06 kg NO_3^--N/(m^3·d) in the early phase of Stage I (day 1–40), the average NO_3^- removal efficiency was only 89.3% (Figure 1a,b). The main reason might be attributed to the low abundance of S^0OB in the inoculation sludge and its slow growth rate, which led to a start-up period of S^0-PBR as long as 28 days [37]. Yang et al. (2016a) [38] mentioned that the volumetric denitrification loading rate was less than 0.1 kg NO_3^--N/(m^3·d) when the MLVSS concentration remained below 0.3 g/L in the anoxic filter. After the adaption period, NO_3^- was occasionally detected in the S^0-PBR effluent during days 40–99 (Figure 1a). The accumulation of functional biomass could explain this result due to the relatively strong biomass retention capacity of packed-bed reactors [39]. The S^0OB could become the dominant microbial community in the S^0-PBR since the absence of organic supplementation.

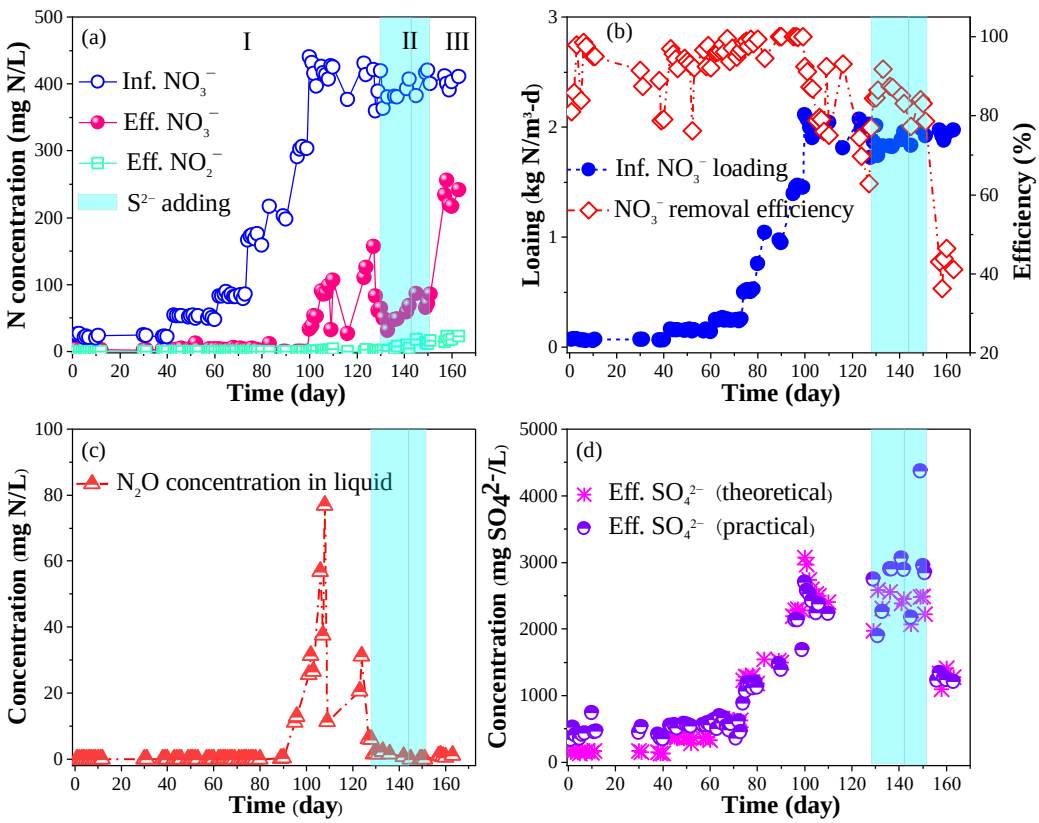

Figure 1. Long-term performance of the S^0-PBR: NO_3^- and NO_2^- concentrations of influent and effluent (**a**), influent NO_3^- loading and NO_3^- removal efficiency variations (**b**), effluent N_2O concentration in liquid (**c**), and theoretical and practical SO_4^{2-} generation (**d**).

Given the limited electron-scavenging capability from the solid S^0 interface by S^0OB [40,41], the NO_3^- reduction rate was significantly higher than the NO_2^- reduction rate, leading to NO_2^- accumulation in the SADN system. However, NO_2^- was

undetectable during days 1–99 (Figure 1a), even during days 95–99, corresponding with a high volumetric loading rate of 1.44 kg NO_3^--N/(m^3·d) and high average NO_3^- removal efficiency of approximately 100% (Figure 1a,b). The efficient denitrification performance of the S^0-PBR could be attributed to the use of smaller S^0 particles (0.5–1 mm) with larger specific surface areas in the S^0-PBR than those in the literature (2–16 mm) [10,32]. The higher surface areas of S^0 improved the mass-transfer efficiency during S^0OB utilization of S^0 [10]. Consequently, the dissolution process of $S_{chem}{}^0$, considered the main rate-limiting step, was largely promoted [10,19,42].

However, during days 100–127, the average effluent NO_3^- concentration increased to 78 mg NO_3^--N/L, and the NO_3^- removal efficiency continuously declined to 62.7% on day 127 (Figure 1a,b). In addition, overloading of the S^0-PBR was evidenced by the detection of NO_2^- and high-level average N_2O concentration of 32 mg N_2O-N/L in the effluent (Figure 1a,c). These could be seen as reliable markers of the reactor overloading in the SADN process [10,43,44]. Therefore, the maximum NO_3^- removal loading rate of the S^0-PBR was considered as 1.44 kg NO_3^--N/(m^3·d) during days 95–99, which was 1.88 times higher than the result obtained by Koenig et al. (2001) [24] who used bigger size of S^0 particles, 2.8–5.6 mm.

Of note, the practical effluent SO_4^{2-} concentration during days 1–40 and 43–60 averaged 447 mg SO_4^{2-}/L and 542 mg SO_4^{2-}/L (Figure 1d), respectively, which were significantly higher than the theoretical values that were 155 mg SO_4^{2-}/L and 364 mg SO_4^{2-}/L. It is well known that the sulfur-based autotrophic disproportionation process occurs only after NO_3^- is depleted in the SADN system [45–47], especially near the effluent side of S^0-PBR [32]. Hijnen et al. (1992) [48] pointed out that the volumetric loading rate of S^0-PBR should be kept above the minimum limitation, 0.22 kg NO_3^--N/(m^3·d), to prevent the head loss caused by the SD process. It was reasonable to infer that the occurrence of the SD process at these two early periods of Stage I, due to the relatively low volumetric loading rates, 0.06–0.15 kg NO_3^--N/(m^3·d), and the nearly complete NO_3^- removal in the S^0-PBR (Figure 1a,b). According to Equation (4), SO_4^{2-} in excess amount of theoretical production in these two periods was likely to come from the SD process. In addition, the ratios of SO_4^{2-} production to NO_3^- removal were becoming closer to the theoretical value as the volumetric loading rate increased (Figure 1d). As NO_3^- loading rates were in the range of 0.76–1.92 kg NO_3^--N/(m^3·d) during days 80–127 (Figure 1b), this ratio was almost equivalent to the theoretical value of 7.54 mg SO_4^{2-}/mg NO_3^--N, suggesting the inhibition of high NO_3^- loading rate on SD process. A previous study also reported that the SD process was completely inhibited when influent NO_3^- loading exceeded 0.72 kg NO_3^--N/(m^3·d) and the concentration of the sulfur-heterologous electron acceptors (e.g., NO_3^-, NO_2^-, and dissolved oxygen) increased to 1.1 mg/L [49].

In Stage II, 30 to 50 mg S/L chemical S^{2-} was added into the S^0-PBR in sequence while keeping the volumetric loading rate constant at about 1.92 kg NO_3^--N/(m^3·d), same as that during days 100–127 in Stage I (Figure 1b). As a result of the addition of 30 mg S^{2-}-S/L, the downward trend of NO_3^- removal efficiency was terminated and replaced by an upward trend during days 128–142, showing that the average NO_3^- removal efficiency was increased to 85.3% from 81.3% (Figure 1b). In addition, upon the overloading of influent NO_3^-, the average N_2O concentration of 2 mg N_2O-N/L in effluent samples was far lower than that during days 100–127 (32 mg N_2O-N/L) without chemical S^{2-} addition, decreasing N_2O accumulation by 93.8%. The result differs from previous points that the S^{2-} could precipitate with soluble copper cofactors in the N_2O reductase, leading to a rise in N_2O production [50]. However, it was also observed in a previous study by Yang et al. (2016) [51] that the bio-poisoning chemical S^{2-} could be instantly oxidized into S_n^{2-} by membrane-bound sulfide-quinine reductase presented in almost S^0OB, and S_n^{2-} acting as a bioavailable electron donor could contribute to N_2O reduction.

However, the average NO_2^- concentration increased from 6 mg NO_2^--N/L to 15 mg NO_2^--N/L during days 145–151 in Stage II, when the dosage increased to 50 mg S^{2-}-S/L. The bioavailability of insoluble $S_{chem}{}^0$ in this S^0-PBR could be greatly improved by

adding a higher S^{2-} concentration to promote the chemical polysulfuration process. The formation of S_n^{2-} and the higher competitive capacity of the nitrate reductase for electrons than nitrite reductase explained well the severe NO_2^- accumulation [52,53]. Moreover, it has been reported that high-level chemical S^{2-} exerted an inhibitory effect on nitrite reductase activity and ceased the NO_2^- reduction process [54–56]. As a result of the severe NO_2^- accumulation, the denitrification microorganisms in the S^0-PBR could be further restrained [41,57,58] and caused an undesirable NO_3^- removal performance, exhibiting the average NO_3^- removal efficiency declined to 80.8% from 85.2% during days 128–142 (Figure 1d).

In Stage III (days 156–163), the operational conditions were identical to those during days 100–127 in Stage I, with an overloading volumetric loading rate of 1.92 kg NO_3^--N/(m^3·d) and no external chemical S^{2-} addition. The average NO_3^- removal efficiency decreased further to 42.1% (Figure 1b). Simultaneously, the NO_2^- accumulation was aggravated to 19 mg NO_2^--N/L (Figure 1a), suggesting the deterioration of SADN performance in the S^0-PBR with high influent NO_3^- loading applied. The high volumetric loading rate completely prevented the SD process in Stage III, as evidenced by the similar practical SO_4^{2-} production (1267 mg SO_4^{2-}/L) and theoretical value (1327 mg SO_4^{2-}/L) (Figure 1d). Therefore, the deterioration could be attributed to the lack of precursor, such as biogenic/chemical S^{2-}, to induce a chemical polysulfuration reaction.

3.2. The Short-Term Effects of Varying S^0 Particle Sizes and Chemical S^{2-} Addition on the SADN Process

Batch experiments were categorized into four groups based on the diameters of S^0 particles, i.e., 1–2 mm, 3–5 mm, 7–9 mm, and 10–12 mm, for evaluating the effect of varying particle sizes on the SADN process.

NO_3^- removal fastened as the S^0 particle size decreased (Figure 2a). NO_3^- was almost completely removed at 12 h when the S^0 size was smaller than 5 mm (Figure 2a). Comparatively, the residual NO_3^- concentrations were approximately 16 mg NO_3^--N/L and 12 mg NO_3^--N/L at 12 h in the groups with the S^0 particle sizes of 10–12 and 7–9 mm, respectively. Meanwhile, as a result of a lower NO_2^- reduction rate and faster NO_3^- reduction rate, the build-up of NO_2^- was gradually formed in all groups (Figure 2b), which was consistent with points that the capability of electron-scavenging for nitrite reductase was weaker than nitrate reductase [59,60].

The average specific NO_3^- removal rates within the first 12 h in groups with S^0 sizes of 10–12 mm, 7–9 mm, 3–5 mm, and 1–2 mm applied were 0.672 g NO_3^--N/g VSS/h, 0.678 g NO_3^--N/g VSS/h, 0.850 g NO_3^--N/g VSS/h, and 0.910 g NO_3^--N/g VSS/h, respectively (Figure 2c). Additionally, it has been reported that a half-order reaction model could be used to explain the kinetics of the SADN process [24]. The half-order kinetic constants in groups with S^0 sizes of 10–12, 7–9, 3–5, and 1–2 mm applied were calculated to be 0.382 mg-$N^{1/2}/L^{1/2}$/h, 0.435 mg-$N^{1/2}/L^{1/2}$/h, 0.545 mg-$N^{1/2}/L^{1/2}$/h, and 0.565 mg-$N^{1/2}/L^{1/2}$/h (Figure 2c), suggesting that the reaction rate constant increased with the specific surface area of S^0 [25]. The smaller S^0 size with a higher specific area not only provided a larger area for biofilm growth but, more importantly, reduced the mass-transfer resistance of insoluble S^0 [10,29].

Generally, it was assumed that the saturation constants K_s was as low as 0.22 mg S/L in the SADN process [24,47], indicating that the affinities between S^0 and the enzymes related in S^0 oxidiation, such as SDO/SOR/Hdr were strong. Given that S^0 was only taken up by S^0OB after its solubilization and diffusion [16,21], the mass-transfer resistance of insoluble S^0 became the main rate-limiting factor in the SADN system. The specific surface area of insoluble sulfur was the key parameter affecting the population of hydrolysis bacteria attached to its surface and the dissolution kinetics [61]. A kinetic model focusing on S^0 hydrolysis as a prior and rate-limiting step was proposed, where both activities of hydrolytic biomass and autotrophic denitrifying bacteria in the SADN process were

considered [19,62]. The model demonstrated that the specific surface area of S^0 was the dominant factor affecting the denitrification rate.

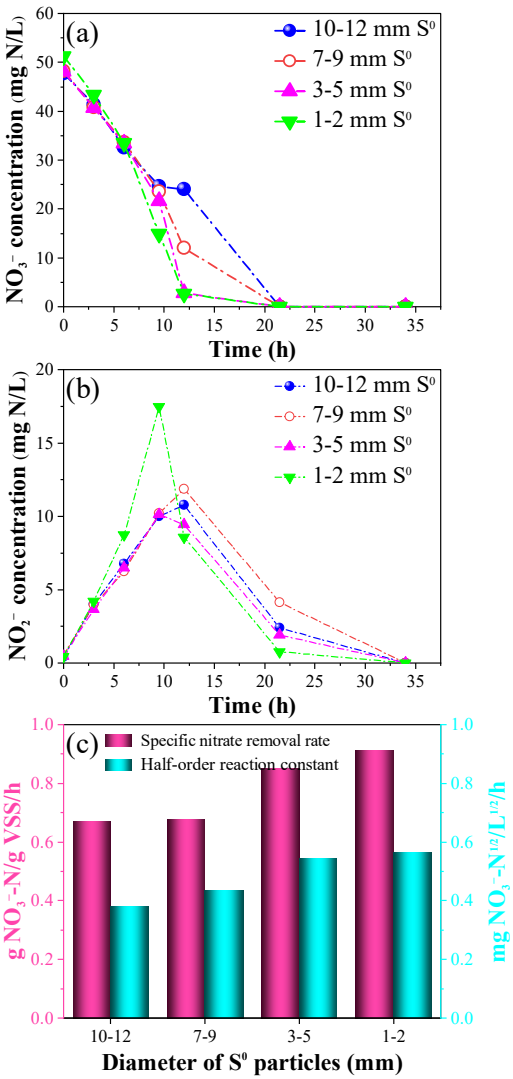

Figure 2. Variations of NO_3^- removal (**a**), NO_2^- accumulation (**b**), specific NO_3^- removal rate, and half-order reaction constant (**c**) with varying S^0 particle size applied.

To investigate how S^{2-} or S_n^{2-} promoted NO_3^- removal, batch Test II with an initial dosage of 20 mg S^{2-}-S/L was conducted. During 0–9.5 h, the specific NO_3^- removal rates and NO_3^- consumption slope k in the S^{2-}-added group were 0.557 g NO_3^--N/g VSS/h and 0.0465 (Figure 3a,b), respectively, significantly higher than the S^{2-}-free group of 0.366 g NO_3^--N/g VSS/h and 0.0364. It could be due to the fact that the lower Gibbs energy was required when S^{2-} with the relatively high solubility served as the additional electron donor, compared with the conventional SADN process [53]. However, the quietly close NO_3^- removal rates (3.0 mg NO_3^--N/(L·d) versus 3.6 mg NO_3^--N/(L·d)) were found in the two groups with S^0 and chemical S^{2-} as a single electron source by Qi et al. (2023) [63]. This result indicated that the acceleration of NO_3^- removal in this study should be mainly attributed to the S_n^{2-} formation instead of chemical S^{2-} participation. In the presence of chemicals S^{2-} and S^0, the abiotic polysulfuration process was triggered (Equation (2)). As a result of the product of soluble S_n^{2-} with higher bioavailability, the NO_3^- removal rate was remarkably enhanced in the S^{2-}-added group. This result was consistent with previous studies [29,30,32] and the improvement in NO_3^- removal efficiency in Stage II (day128–142) in the S^0-PBR.

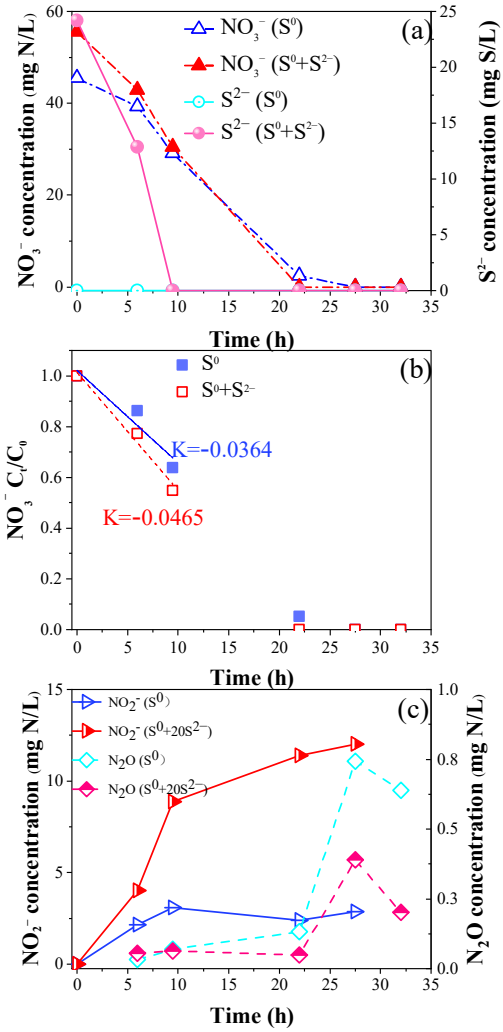

Figure 3. Variations of NO_3^- and S^{2-} (**a**), NO_3^- consumptions kinetics (**b**), and NO_2^- and N_2O accumulation (**c**) over time in batch tests with and without the addition chemical S^{2-}.

Of note, NO_2^- accumulation occurred in both groups and was aggravated by S^{2-} addition (Figure 3c). The results were similar to the long-term performance of S^0-PBR in Stage II and the previous study [63,64], indicating that dosing chemical S^{2-} could significantly improve the NO_3^- reduction process but rarely promote NO_2^- reduction process. The aggravated NO_2^- accumulation in the S^{2-}-added group resulted from the imbalance rate of the NO_3^- and NO_2^- reduction process, and the imbalance could be attributed to two main reasons. Firstly, the extent of NO_2^- accumulation was positively correlated with the NO_3^- reduction rate [60]. It can also be noticed that the NO_3^- removal rate was faster in the S^{2-}-added group (Figure 3a,b) due to the presence of S_n^{2-}, which explained the severe NO_2^- accumulation well. Secondly, the bio-toxicity of chemical S^{2-} to nitrite reductase [54,55] and the higher competitive capacity of the nitrate reductase for electrons both hindered the NO_2^- reduction process [54–56].

Additionally, in the S^{2-}-free group, only 1.6% of removed NO_3^--N was in the form of N_2O-N within 27.5 h. The amount of N_2O production was much lower than in the HD process, suggesting that less N_2O was produced in the SADN process [19,65]. Additionally, a further decrease in N_2O production in the S^{2-}-added group was observed even in the presence of higher NO_2^- accumulation, only accounting for 0.7% of removed NO_3^--N within 27.5 h (Figure 3c). The result was consistent with the performance of the S^0-PBR (Figure 1c) in Stage II. Similarly, a linearly proportional relationship between chemical S^{2-} concentration and N_2O emissions during autotrophic denitrification was reported in the

study, including the mass ratio of S^{2-}-S:NO_3^--N up to 5 [51]. Yang et al. (2016b) [51] also confirmed that chemical S^{2-} had no inhibitory effect on nitrous oxide reductase. Moreover, S_n^{2-} was formed in the S^{2-}-added group due to the abiotic polysulfuration process. When S_n^{2-} participated in the N_2O reduction process, higher energy than S^0-oxidation was yielded [66]. These explained the lower N_2O production in the S^{2-}-added group well.

4. Conclusions

Based on the long-term performance of the S^0-PBR, the NO_3^- removal loading rate could be significantly enhanced using smaller S^0 particle fillers with a higher specific surface area. More importantly, chemical S^{2-} supplementation improved the performance of the S^0-PBR under overloading conditions. It proved the feasibility of establishing an in situ PiSADN system by adding chemical S^{2-} directly for high-loading wastewater treatment. The conducted batch tests have clarified the kinetic dynamics between the sizes of S^0 particles and the rate of denitrification. Furthermore, the responses of the SADN process to chemical S^{2-} were also investigated. The principle findings were summarized as follows:

- Utilization of smaller S^0 particles (0.5–1 mm) within the S^0-PBR achieved a high volumetric loading rate of 1.44 kg NO_3^--N/(m^3·d) and a NO_3^- removal efficiency nearing 100%, significantly surpassing outcomes observed in S^0-PBR employing larger S^0 particles (2–16 mm);
- The supplementation of 30 mg S^{2-}-S/L in the S^0-PBR led to an increase in NO_3^- removal efficiency from 81.3%% to 85.3% and facilitated a 93.8% reduction in N_2O accumulation;
- In the batch tests with a S^0 size of 10–12, 7–9, 3–5, and 1–2 mm applied, the average specific NO_3^- removal rates were 0.672 g NO_3^--N/g VSS/h, 0.678 g NO_3^--N/g VSS/h, 0.850 g NO_3^--N/g VSS/h, and 0.910 g NO_3^--N/g VSS/h, respectively, while the half-order kinetic constants were 0.382 mg-$N^{1/2}/L^{1/2}$/h, 0.435 mg-$N^{1/2}/L^{1/2}$/h, 0.545 mg-$N^{1/2}/L^{1/2}$/h, and 0.565 mg-$N^{1/2}/L^{1/2}$/h, respectively;
- The specific NO_3^- removal rates and NO_3^- consumption slope k in the S^{2-}-added group were 0.557 g NO_3^--N/g VSS/h and 0.0465, respectively, significantly higher than S^{2-}-free group of 0.366 g NO_3^--N/g VSS/h and 0.0364;
- The 1.6% of removed NO_3^--N was in the form of N_2O within 27.5 h in the S^{2-}-free group, while only 0.7% of the removed NO_3^--N was produced as N_2O in the S^{2-}-added group.

Author Contributions: Formal analysis, Conceptualization, Methodology, Investigation, Writing—original draft, J.X.; Investigation, Writing—review & editing, Z.L.; Supervision, Methodology, Funding acquisition, Y.X.; Supervision, Investigation, Methodology, Writing—review & editing, C.L.; Supervision, Investigation, Conceptualization, Project administration, Funding acquisition, Writing—review & editing, L.P. All authors have read and agreed to the published version of the manuscript.

Funding: This research was funded by National Natural Science Foundation of China (No. 52100061) and the Hubei Provincial Key Research and Development Program (No. 2022BCA067).

Data Availability Statement: Data will be made available on request.

Acknowledgments: The authors are grateful for the research collaboration.

Conflicts of Interest: The authors declare no conflict of interest.

References

1. Liu, H.; Jiang, W.; Wan, D.; Qu, J. Study of a combined heterotrophic and sulfur autotrophic denitrification technology for removal of nitrate in water. *J. Hazard. Mater.* **2009**, *169*, 23–28. [CrossRef]
2. Zhang, X.; Zhang, Y.; Shi, P.; Bi, Z.; Shan, Z.; Ren, L. The deep challenge of nitrate pollution in river water of China. *Sci. Total Environ.* **2021**, *770*, 144674. [CrossRef] [PubMed]
3. Danni, S.O.; Bouchaou, L.; Elmouden, A.; Brahim, Y.A.; N'da, B. Assessment of water quality and nitrate source in the Massa catchment (Morocco) using δ 15N and δ 18O tracers. *Appl. Radiat. Isot.* **2019**, *154*, 108859. [CrossRef] [PubMed]

4. Fields, S. Global Nitrogen: Cycling out of Control. *Environ. Health Perspect.* **2004**, *112*, A556–A563. [CrossRef]
5. Della Rocca, C.; Belgiorno, V.; Meriç, S. Overview of in-situ applicable nitrate removal processes. *Desalination* **2007**, *204*, 46–62. [CrossRef]
6. Panda, B.; Chidambaram, S.; Snow, D.; Malakar, A.; Singh, D.K.; Ramanathan, A.L. Source apportionment and health risk assessment of nitrate in foothill aquifers of Western Ghats, South India. *Ecotoxicol. Environ. Saf.* **2022**, *229*, 113075. [CrossRef] [PubMed]
7. Sahinkaya, E.; Dursun, N. Sulfur-oxidizing autotrophic and mixotrophic denitrification processes for drinking water treatment: Elimination of excess sulfate production and alkalinity requirement. *Chemosphere* **2012**, *89*, 144–149. [CrossRef]
8. Zumft, W.G. Cell biology and molecular basis of denitrification. *Microbiol. Mol. Biol. Rev.* **1997**, *61*, 533–616.
9. Oh, S.E.; Yoo, Y.B.; Young, J.C.; Kim, I.S. Effect of organics on sulfur-utilizing autotrophic denitrification under mixotrophic conditions. *J. Biotechnol.* **2001**, *92*, 1–8. [CrossRef]
10. Sierra-Alvarez, R.; Beristain-Cardoso, R.; Salazar, M.; Gómez, J.; Razo-Flores, E.; Field, J.A. Chemolithotrophic denitrification with elemental sulfur for groundwater treatment. *Water Res.* **2007**, *41*, 1253–1262. [CrossRef]
11. Claus, G.N.; Kutzner, H.R. Physiology and kinetics of autotrophic denitrification by Thiobacillus denitrificans. *Appl. Microbiol. Biotechnol.* **1985**, *22*, 283–288. [CrossRef]
12. Wiesmann, U. Biological nitrogen removal from wastewater. *Adv. Biochem. Eng. Biotechnol.* **1994**, *51*, 113–154.
13. Lee, K.-C.; Rittmann, B.E. Applying a novel autohydrogenotrophic hollow-fiber membrane biofilm reactor for denitrification of drinking water. *Water Res.* **2002**, *36*, 2040–2052. [CrossRef]
14. Batchelor, B.; Lawrence, A.W. Autotrophic denitrification using elemental sulfur. *Water Pollut. Control Fed.* **1978**, *50*, 1986–2001.
15. Soares, M.I.M. Denitrification of groundwater with elemental sulfur. *Water Res.* **2002**, *36*, 1392–1395. [CrossRef]
16. Wang, Y.; Bott, C.; Nerenberg, R. Sulfur-based denitrification: Effect of biofilm development on denitrification fluxes. *Water Res.* **2016**, *100*, 184–193. [CrossRef]
17. Cui, Y.-X.; Biswal, B.K.; Guo, G.; Deng, Y.-F.; Huang, H.; Chen, G.-H.; Wu, D. Biological nitrogen removal from wastewater using sulphur-driven autotrophic denitrification. *Appl. Microbiol. Biotechnol.* **2019**, *103*, 6023–6039. [CrossRef]
18. Peng, L.; Ni, B.-J.; Erler, D.; Ye, L.; Yuan, Z. The effect of dissolved oxygen on N_2O production by ammonia-oxidizing bacteria in an enriched nitrifying sludge. *Water Res.* **2014**, *66*, 12–21. [CrossRef]
19. Kostrytsia, A.; Papirio, S.; Frunzo, L.; Mattei, M.R.; Porca, E.; Collins, G.; Lens, P.N.L.; Esposito, G. Elemental sulfur-based autotrophic denitrification and denitritation: Microbially catalyzed sulfur hydrolysis and nitrogen conversions. *J. Environ. Manag.* **2018**, *211*, 313–322. [CrossRef]
20. Florentino, A.P.; Weijma, J.; Stams, A.J.M.; Sánchez-Andrea, I. Ecophysiology and Application of Acidophilic Sulfur-Reducing Microorganisms. In *Biotechnology of Extremophiles*; Springer: Berlin/Heidelberg, Germany, 2016; pp. 141–175.
21. Moraes, B.S.; Foresti, E. Determination of the intrinsic kinetic parameters of sulfide-oxidizing autotrophic denitrification in differential reactors containing immobilized biomass. *Bioresour. Technol.* **2012**, *104*, 250–256. [CrossRef] [PubMed]
22. Batchelor, B.; Lawrence, A.W. A kinetic model for autotrophic denitrification using elemental sulfur. *Water Res.* **1978**, *12*, 1075–1084. [CrossRef]
23. Dong, H.; Sun, Y.-L.; Sun, Q.; Zhang, X.-N.; Wang, H.-C.; Wang, A.-J.; Cheng, H.-Y. Effect of sulfur particle morphology on the performance of element sulfur-based denitrification packed-bed reactor. *Bioresour. Technol.* **2023**, *367*, 128238. [CrossRef]
24. Koenig, A.; Liu, L.H. Kinetic model of autotrophic denitrification in sulfur packed-bed reactors. *Water Res.* **2001**, *35*, 1969–1978. [CrossRef] [PubMed]
25. Moon, H.S.; Chang, S.W.; Nam, K.; Choe, J.; Kim, J.Y. Effect of reactive media composition and co-contaminants on sulfur-based autotrophic denitrification. *Environ. Pollut.* **2006**, *144*, 802–807. [CrossRef]
26. Florentino, A.P.; Jan, W.; Stams, A.J.M.; Sánchez-Andrea, I. Sulfur Reduction in Acid Rock Drainage Environments. *Environ. Sci. Technol.* **2015**, *49*, 11746–11755. [CrossRef] [PubMed]
27. Ucar, D.; Yilmaz, T.; Di Capua, F.; Esposito, G.; Sahinkaya, E. Comparison of biogenic and chemical sulfur as electron donors for autotrophic denitrification in sulfur-fed membrane bioreactor (SMBR). *Bioresour. Technol.* **2020**, *299*, 122574. [CrossRef]
28. Wang, Y.; Sabba, F.; Bott, C.; Nerenberg, R. Using Kinetics and Modeling to Predict Denitrification Fluxes in Elemental-Sulfur Based Biofilms. *Biotechnol. Bioeng.* **2019**, *116*, 2698–2709. [CrossRef]
29. Zhang, L.; Qiu, Y.-Y.; Zhou, Y.; Chen, G.-H.; van Loosdrecht, M.C.M.; Jiang, F. Elemental sulfur as electron donor and/or acceptor: Mechanisms, applications and perspectives for biological water and wastewater treatment. *Water Res.* **2021**, *202*, 117373. [CrossRef]
30. Qiu, Y.-Y.; Zhang, L.; Mu, X.; Li, G.; Guan, X.; Hong, J.; Jiang, F. Overlooked pathways of denitrification in a sulfur-based denitrification system with organic supplementation. *Water Res.* **2020**, *169*, 115084. [CrossRef]
31. Zhang, L.; Zhang, C.; Hu, C.; Liu, H.; Bai, Y.; Qu, J. Sulfur-based mixotrophic denitrification corresponding to different electron donors and microbial profiling in anoxic fluidized-bed membrane bioreactors. *Water Res.* **2015**, *85*, 422–431. [CrossRef]
32. Qiu, Y.-Y.; Gong, X.; Zhang, L.; Zhou, S.; Li, G.; Jiang, F. Achieving a Novel Polysulfide-Involved Sulfur-Based Autotrophic Denitrification Process for High-Rate Nitrogen Removal in Elemental Sulfur-Packed Bed Reactors. *ACS EST Eng.* **2022**, *2*, 1504–1513. [CrossRef]
33. Finster, K. Microbiological disproportionation of inorganic sulfur compounds. *J. Sulfur Chem.* **2008**, *29*, 281–292. [CrossRef]

34. American Public Health Association (APHA); American Water Works Association (AWWA); Water Environment Federation (AEF). *Standard Methods for the Examination of Water and Wastewater*; American Public Health Association (APHA): Washington, DC, USA, 2005.
35. Kleinjan, W.E.; de Keizer, A.; Janssen, A.J.H. Equilibrium of the reaction between dissolved sodium sulfide and biologically produced sulfur. *Colloids Surf. B Biointerfaces* **2005**, *43*, 228–237. [CrossRef]
36. Zhang, L.; Zhang, Z.; Sun, R.; Liang, S.; Chen, G.-H.; Jiang, F. Self-accelerating sulfur reduction via polysulfide to realize a high-rate sulfidogenic reactor for wastewater treatment. *Water Res.* **2018**, *130*, 161–167. [CrossRef]
37. Hao, W.; Li, Q.; Liu, P.; Han, J.; Duan, R.; Liang, P. A new inoculation method of sulfur autotrophic denitrification reactor for accelerated start-up and better low-temperature adaption. *Sci. Total Environ.* **2022**, *823*, 153657. [CrossRef]
38. Yang, W.; Lu, H.; Khanal, S.K.; Zhao, Q.; Meng, L.; Chen, G.-H. Granulation of sulfur-oxidizing bacteria for autotrophic denitrification. *Water Res.* **2016**, *104*, 507–519. [CrossRef]
39. Ruan, Y.-J.; Luo, G.-Z.; Tan, H.-X.; Che, X.; Jiang, Y.; Sun, D.-C. Nitrate and phosphate removal in sulphur-coral stone autotrophic denitrification packed-bed reactors. *J. Environ. Eng. Sci.* **2013**, *8*, 267–276. [CrossRef]
40. Sadeq, M.; Moe, C.L.; Attarassi, B.; Cherkaoui, I.; ElAouad, R.; Idrissi, L. Drinking water nitrate and prevalence of methemoglobinemia among infants and children aged 1–7 years in Moroccan areas. *Int. J. Hyg. Environ. Health* **2008**, *211*, 546–554. [CrossRef]
41. Chen, F.; Li, X.; Gu, C.; Huang, Y.; Yuan, Y. Selectivity control of nitrite and nitrate with the reaction of S^0 and achieved nitrite accumulation in the sulfur autotrophic denitrification process. *Bioresour. Technol.* **2018**, *266*, 211–219. [CrossRef]
42. Vavilin, V.A.; Fernandez, B.; Palatsi, J.; Flotats, X. Hydrolysis kinetics in anaerobic degradation of particulate organic material: An overview. *Waste Manag.* **2008**, *28*, 939–951. [CrossRef] [PubMed]
43. Flere, J.M.; Zhang, T.C. Nitrate Removal with Sulfur-Limestone Autotrophic Denitrification Processes. *J. Environ. Eng.* **1999**, *125*, 721–729. [CrossRef]
44. Lu, H.; Chandran, K. Factors promoting emissions of nitrous oxide and nitric oxide from denitrifying sequencing batch reactors operated with methanol and ethanol as electron donors. *Biotechnol. Bioeng.* **2010**, *106*, 390–398. [CrossRef]
45. Sahu, A.; Conneely, T.; Nüsslein, K.; Ergas, S. Biological Perchlorate Reduction in Packed Bed Reactors Using Elemental Sulfur. *Environ. Sci. Technol.* **2009**, *43*, 4466–4471. [CrossRef]
46. Wan, D.; Li, Q.; Liu, Y.; Xiao, S.; Wang, H. Simultaneous reduction of perchlorate and nitrate in a combined heterotrophic-sulfur-autotrophic system: Secondary pollution control, pH balance and microbial community analysis. *Water Res.* **2019**, *165*, 115004. [CrossRef]
47. Guo, G.; Li, Z.; Chen, L.; Ling, Q.; Zan, F.; Isawi, H.; Hao, T.; Ma, J.; Wang, Z.; Chen, G.H.; et al. Advances in elemental sulfur-driven bioprocesses for wastewater treatment: From metabolic study to application. *Water Res.* **2022**, *213*, 118143. [CrossRef]
48. Hijnen, W.; Bennekom, C.A.; Mijnarends, B.J. Optimization of the sulphur-limestone filtration process for nitrate removal from groundwater. *Aqua* **1992**, *41*, 209–218.
49. Sun, Y.-L.; Zhai, S.; Qian, Z.-M.; Yi, S.; Zhuang, W.-Q.; Cheng, H.-Y.; Zhang, X.; Wang, A.-J. Managing Microbial Sulfur Disproportionation for Optimal Sulfur Autotrophic Denitrification in a Pilot-scale Elemental Sulfur Packed-bed Reactor. *Water Res.* **2023**, *243*, 120356. [CrossRef]
50. Richardson, D.; Felgate, H.; Watmough, N.; Thomson, A.; Baggs, E. Mitigating release of the potent greenhouse gas N_2O from the nitrogen cycle—Could enzymic regulation hold the key? *Trends Biotechnol.* **2009**, *27*, 388–397. [CrossRef]
51. Yang, W.; Zhao, Q.; Lu, H.; Ding, Z.; Meng, L.; Chen, G.-H. Sulfide-driven autotrophic denitrification significantly reduces N_2O emissions. *Water Res.* **2016**, *90*, 176–184. [CrossRef]
52. Liu, Y.; Peng, L.; Ngo, H.; Guo, W.; Wang, D.-B.; Pan, Y.; Sun, J.; Ni, B.-J. Evaluation of Nitrous Oxide Emission from Sulfide- and Sulfur-Based Autotrophic Denitrification Processes. *Environ. Sci. Technol.* **2016**, *50*, 9407–9415. [CrossRef] [PubMed]
53. Lin, S.; Mackey, H.; Hao, T.; Guo, G.; Loosdrecht, M.; Chen, G.H. Biological Sulfur Oxidation in Wastewater Treatment: A Review of Emerging Opportunities. *Water Res.* **2018**, *143*, 399–415. [CrossRef] [PubMed]
54. Beristain-Cardoso, R.; Sierra-Alvarez, R.; Rowlette, P.; Razo-Flores, E.; Gomez, J.; Field, J. Sulfide oxidation under chemolithoautotrophic denitrifying conditions. *Biotechnol. Bioeng.* **2006**, *95*, 1148–1157. [CrossRef]
55. Lu, H.; Huang, H.; Yang, W.; Mackey, H.; Khanal, S.; Wu, D.; Chen, G.-H. Elucidating the stimulatory and inhibitory effects of dissolved sulfide on sulfur-oxidizing bacteria (SOB) driven autotrophic denitrification. *Water Res.* **2018**, *133*, 165–172. [CrossRef]
56. Huang, S.; Yu, D.; Chen, G.; Wang, Y.; Tang, P.; Liu, C.; Tian, Y.; Zhang, M. Realization of nitrite accumulation in a sulfide-driven autotrophic denitrification process: Simultaneous nitrate and sulfur removal. *Chemosphere* **2021**, *278*, 130413. [CrossRef]
57. An, S.; Tang, K.; Nemati, M. Simultaneous biodesulphurization and denitrification using an oil reservoir microbial culture: Effects of sulphide loading rate and sulphide to nitrate loading ratio. *Water Res.* **2010**, *44*, 1531–1541. [CrossRef]
58. Zhou, Z.; Xing, C.; An, Y.; Hu, D.; Qiao, W.; Wang, L. Inhibitory effects of sulfide on nitrifying biomass in the anaerobic–anoxic–aerobic wastewater treatment process. *J. Chem. Technol. Biotechnol.* **2014**, *89*, 214–219. [CrossRef]
59. Di Capua, F.; Pirozzi, F.; Lens, P.N.L.; Esposito, G. Electron donors for autotrophic denitrification. *Chem. Eng. J.* **2019**, *362*, 922–937. [CrossRef]

60. Bao, H.-X.; Li, Z.-R.; Song, Z.-B.; Wang, A.-J.; Zhang, X.-N.; Qian, Z.-M.; Sun, Y.-L.; Cheng, H.-Y. Mitigating nitrite accumulation during S^0-based autotrophic denitrification: Balancing nitrate-nitrite reduction rate with thiosulfate as external electron donor. *Environ. Res.* **2022**, *204*, 112016. [CrossRef]
61. Esposito, G.; Frunzo, L.; Panico, A.; Pirozzi, F. Modelling the effect of the OLR and OFMSW particle size on the performances of an anaerobic co-digestion reactor. *Process Biochem.* **2011**, *46*, 557–565. [CrossRef]
62. Kostrytsia, A.; Papirio, S.; Mattei, M.; Frunzo, L.; Lens, P.N.L.; Esposito, G. Sensitivity analysis for an elemental sulfur-based two-step denitrification model. *Water Sci. Technol.* **2018**, *78*, 1296–1303. [CrossRef] [PubMed]
63. Qi, X.; Han, J.; Kou, Z.; Liang, P. Supplementary sulfide during inoculation for improved sulfur autotrophic denitrification performance and adaptation to low temperature. *Sci. Total Environ.* **2023**, *900*, 166365. [CrossRef] [PubMed]
64. Bao, H.-X.; Wang, H.-L.; Wang, S.-T.; Sun, Y.-L.; Zhang, X.-N.; Cheng, H.-Y.; Qian, Z.-M.; Wang, A.-J. Response of sulfur-metabolizing biofilm to external sulfide in element sulfur-based denitrification packed-bed reactor. *Environ. Res.* **2023**, *231*, 116061. [CrossRef] [PubMed]
65. Zhou, W.; Liu, X.; Dong, X.; Wang, Z.; Yuan, Y.; Wang, H.; He, S. Sulfur-based autotrophic denitrification from the micro-polluted water. *J. Environ. Sci.* **2016**, *44*, 180–188. [CrossRef] [PubMed]
66. Pokorna, D.; Zabranska, J. Sulfur-oxidizing bacteria in environmental technology. *Biotechnol. Adv.* **2015**, *33*, 1246–1259. [CrossRef]